The interface screening model as origin of imprint in $PbZr_xTi_{1-x}O_3$ thin films. II. Numerical simulation and verification

M. Grossmann, O. Lohse, D. Bolten, and U. Boettger
Institut für Werkstoffe der Elektrotechnik, RWTH Aachen, D-52056 Aachen, Germany

R. Waser
Institut für Werkstoffe der Elektrotechnik, RWTH Aachen, D-52056 Aachen, Germany and Institut für Festkörperforschung, Research Center Jülich, D-52425 Jülich, Germany

(Received 26 September 2001; accepted for publication 12 June 2002)

In this article, the interface screening model is theoretically discussed which explains imprint in ferroelectric thin films caused by a large electric field within a surface layer with deteriorated ferroelectric properties. During aging this field is gradually screened by electronic charges. Different screening mechanisms such as charge injection from the electrodes into the film as well as charge separation within the surface layer are considered by implementing a numerical simulation based on the different screening mechanisms. A comparison between experimental and simulation results is presented. The best agreement between experiment and simulation is obtained for a Frenkel–Poole type charge separation mechanism within the surface layer. The simulation results indicate relatively shallow trap states (0.35 eV) and a surface layer extension of approximately 5 nm.
 [DOI: 10.1063/1.1498967]

I. INTRODUCTION

Imprint is an important aging mechanism of ferroelectric thin films in view of memory applications[1–3] which manifests itself by a voltage shift of the hysteresis loop. In recent years, many investigations focused on the understanding of the imprint mechanism in order to improve the imprint behavior of ferroelectric thin films. In Ref. 4 the interface screening model has been introduced as a qualitative imprint model which explains imprint to be caused by an electric field E_{if} within a thin surface layer with deteriorated ferroelectric properties. The aim of this article is to refine the interface screening model in order to allow a quantitative description of the imprint behavior in ferroelectric thin films.

According to the proposed model, the field E_{if} in the surface layer (see Fig. 1) is responsible for the transport of electronic charges within the surface layer giving rise to a space charge ρ_x. In the course of aging, these charges are assumed to become trapped at the interface between surface and ferroelectric layer and form σ_{if} [see Fig. 2(a)]. If the detrapping time constant of these trapped charges, σ_{if}, exceeds the ferroelectric switching time by far, these charges remain in their position after the ferroelectric has been switched, and hence, they can be responsible for the voltage shift, $V_{c,\mathrm{shift}}$, of the hysteresis loop characteristic for imprint.

Some evidence has been reported in the literature which explains experimental observations with the existence of such surface traps. Mihara and Stolichnov attribute the leakage conduction behavior of ferroelectric thin films to the entrapment of injected electronic charges at the surface region.[5–7] With the same explanation, Chen interprets the change of the $C-V$ behavior in $Pb(Zr,Ti)O_3$ PZT films caused by an application of a dc bias.[8] As for the physical origin of these trap states, valency changes of regular ions[9–11] or of defect sites such as lead vacancies in PZT[5,6] or Bi excess in $SrBi_2Ta_2O_9$[12] are proposed.

II. INTERFACE SCREENING MODEL

In order to achieve the quantitative description of the imprint behavior the approach is as follows: In a first step, a correlation between the trapped interface charges σ_{if} and the voltage shift of the hysteresis loop $V_{c,\mathrm{shift}}$ is established. Then, different screening mechanisms to generate the trapped interface charges σ_{if} will be discussed. Basically, two different types of screening mechanisms are conceivable. First, E_{if} can cause charge injection from the electrode into the thin film and second, E_{if} can be responsible for charge separation within the surface layer. These screening mechanisms will be discussed in detail. By using the corresponding charge transport expressions, a numerical simulation can be implemented which allows a comparison between the simulation and the experimental results. The sample preparation and the experimental procedures are described in Ref. 4.

A. Correlation between trapped interface charges σ_{if} and $V_{c,\mathrm{shift}}$

Figure 2(a) illustrates an imprinted capacitor with trapped interface charges σ_{if} at the interface between ferroelectric and surface layer and a space charge ρ_x within the surface layer. In addition to the trapped interface charges, the external screening charges σ_0 on the bottom and top electrode have been changed by $\Delta\sigma_1$ and $\Delta\sigma_2$, respectively. The changes of the external screening charges $\Delta\sigma_1$ and $\Delta\sigma_2$ represent a different screening condition in the imprinted state. In the imprinted state, a part of the ferroelectric polarization is screened by the interface charges σ_{if}. In order to account for the different screening condition, charges can flow to and

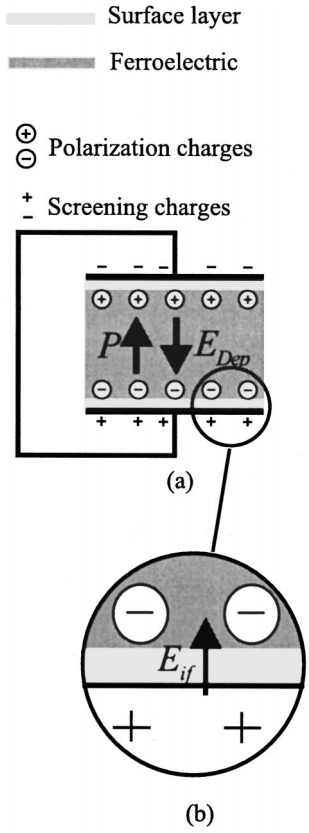

FIG. 1. Sketch of a ferroelectric with a thin surface layer at the electrode interface. Enlargement of the interfacial region shows the driving force of the interface screening model E_{if} in the surface layer.

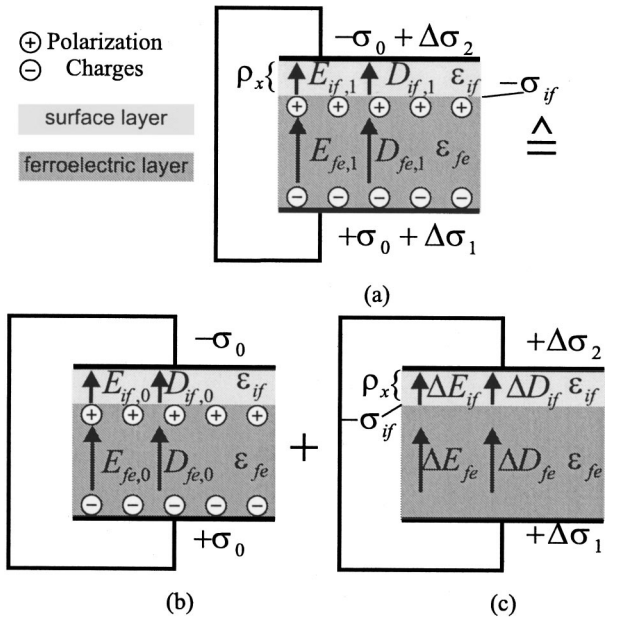

FIG. 2. (a) Aged capacitor structure with trapped interface charges σ_{if}, space charge ρ_x within the surface layer, and a modification of the external screening conditions $\Delta\sigma_1$ and $\Delta\sigma_2$. The aged structure is separated by the superimposition method into the virgin structure (b) and a structure which represents only the changes caused by imprint.

off the electrodes via the external short circuit. This change of the screening charges is described by $\Delta\sigma_1$ and $\Delta\sigma_2$.

The imprinted state illustrated in Fig. 2(a) can be treated by a superimposition method. The imprinted capacitor can be separated into a capacitor identical to the virgin state [see Fig. 2(b)] superimposed to a capacitor which includes only the changes caused by imprint [Fig. 2(c)]. The virgin state capacitor in Fig. 2(b) obeys the same conditions as discussed in Ref. 4 (Fig. 12 therein).

Since the Maxwell equations

$$\mathrm{rot}\,\mathbf{E}=0, \tag{1}$$

$$\mathrm{div}\,\mathbf{D}=\rho \tag{2}$$

are fulfilled for both situations at any position [for virgin state, Fig. 2(b) as well as for the state of changes Fig. 2(c)] the two capacitors can be treated separately.

Figure 2(c) represents a quite stable condition if the detrapping time constant for σ_{if} exceeds the switching time of the ferroelectric by far. Hence, after switching the ferroelectric polarization all polarization charges and external screening charges of the virgin part [Fig. 2(b)] instantaneously reverse their sign. The trapped charges, σ_{if}, however, remain in their position and the resulting field in the interior of the ferroelectric ΔE_{fe} tends to hold the polarization in the previous state. This fact manifests itself as a shift of the hysteresis loop. The voltage shift amounts to

$$V_{c,\mathrm{shift}}=\Delta E_{\mathrm{fe}}(d-\delta), \tag{3}$$

where δ is the extension of the surface layer and d the total film thickness. The change of field can be determined with the dielectric constant in the surface and ferroelectric layer, respectively,

$$\Delta E_j=\frac{\Delta D_j}{\epsilon_0\cdot\epsilon_j} \tag{4}$$

with $j=\mathrm{fe}$ for $x\leqslant d-\delta$ and $j=if$ for $d-\delta<x<d$. In the following, the correlation between $V_{c,\mathrm{shift}}$ and σ_{if} is theoretically derived based on the Maxwell equations, first for the charge separation case.

For the charge separation approach, the field E_{if} causes detrapping of electronic charges within the surface layer which form ρ_x. These charges become trapped at the interface between regular ferroelectric and surface layer (σ_{if}). Since in this case, the trapped interface charges σ_{if} are completely generated by the space charges ρ_x, the space charge layer and the trapped interface charges are correlated as follows:

$$\int_{d-\delta}^{d}\rho_x\,dx=\sigma_{if}. \tag{5}$$

Since the trapped charges σ_{if} change the initial screening condition, changes of the external screening charges $\Delta\sigma_1$ and $\Delta\sigma_2$ have to be taken into account. $\Delta\sigma_1$ and $\Delta\sigma_2$ represent the charges which flow to and off the electrodes via the short circuit in order to meet the screening requirement. According to Eq. (2) the charges have to fulfill

$$\Delta\sigma_1+\int_{d-\delta}^{d}\rho_x\,dx=\Delta\sigma_2+\sigma_{if} \tag{6}$$

and with Eq. (5) also $\Delta\sigma_1=\Delta\sigma_2$ with

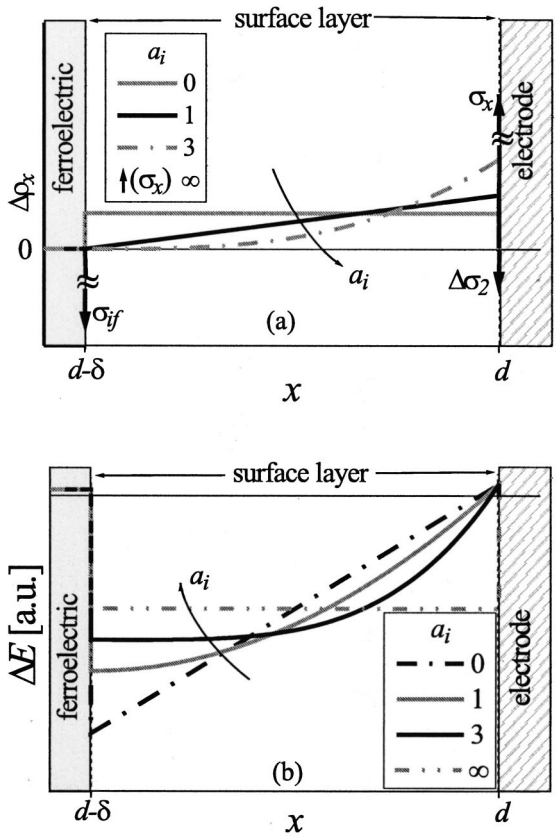

FIG. 3. (a) Variation of the space charge profile within the surface layer according to Eq. (10) as a function of the exponent a_i. (b) The resulting change of the electric field ΔE within the surface layer for four different exponents a_i: $a_i=0$, homogenous space charge distributions and $a_i=1$, $a_i=3$, and $a_i\rightarrow\infty$ representing different levels of space charge accumulation at the electrode.

$$\Delta D_{\mathrm{fe}}=\Delta\sigma_1. \tag{7}$$

Combining the Maxwell equations [Eqs. (1) and (2)] at a position within the surface layer ($d-\delta<x<d$):

$$\Delta E_{\mathrm{fe}}(d-\delta)=-\Delta E_{if}\delta, \tag{8}$$

$$\mathrm{div}\,\Delta D(x)=\rho_x(x), \tag{9}$$

with $\Delta D(x=d-\delta)=\sigma_1-\sigma_{if}$ an additional correlation between σ_{if} and σ_1 can be established that depends on the space charge profile ρ_x.

In order to investigate the influence of the profile of ρ_x on the correlation between σ_{if} and $V_{c,\mathrm{shift}}$, the following power law approach for ρ_x has been evaluated. Different space charge profiles $\rho_x(x)$ have been evaluated in Fig. 3(a): (i) $\rho_{x,1}\sim x^0=\mathrm{const}$, (ii) $\rho_{x,2}\sim x^1$, (iii) $\rho_{x,3}\sim x^3$, and (iv) $\rho_{x,4}\sim x^{\infty}$. The space charge profiles within the surface layer can be expressed as

$$\rho_{x,i}(x)=c_i[x-(d-\delta)]^{a_i} \tag{10}$$

with $a_i=0$, 1, 3, ∞ and $c_i=\mathrm{const}$. Note that c_i is a scaling factor in order to fulfill Eq. (5). The power law approach evaluates a space charge accumulation at the electrode interface. With increasing exponent a_i the space charge accumulates close to the electrode. Using the set of equations introduced above, a correlation between σ_{if} and σ_1 is obtained which depends on the exponent a_i:

$$\Delta\sigma_1=\frac{a_i+1}{a_i+2}\,\frac{C_{\mathrm{fe}}}{C_{\mathrm{fe}}+C_{if}}\,\sigma_{if}, \tag{11}$$

where C_{fe} and C_{if} are the capacitance in the ferroelectric and surface layer, respectively, [$C_{\mathrm{fe}}=\epsilon_0\epsilon_{\mathrm{fe}}(d-\delta)/A$ and $C_{if}=\epsilon_0\epsilon_{if}\delta/A$]. Combining Eqs. (3), (4), (7) and (11) the correlation between the voltage shift of the hysteresis loop, $V_{c,\mathrm{shift}}$, and the trapped interface charges, σ_{if} can be established:

$$V_{c,\mathrm{shift}}=\frac{a_i+1}{a_i+2}\,\frac{A}{C_{\mathrm{fe}}+C_{if}}\,\sigma_{if}. \tag{12}$$

In Fig. 3(b) the influence of the space charge profile on the field lowering ΔE_j ($j=\mathrm{fe}$ for $x\leqslant d-\delta$ and $j=if$ for $d-\delta<x<d$) in the surface layer is plotted for different values of a_i. Note that the initial field, E_{if}, within the surface layer is diminished by ΔE_{if} in the course of aging. Figure 3(b) demonstrates that the space charge profile strongly influences the field lowering ΔE_{if}. For a homogeneous space charge distribution the field lowering ΔE_{if} is most pronounced at the interface between surface layer and ferroelectric which should result in a higher charge separation rate near the electrode-surface-layer interface ($x\rightarrow d$).

However, for increasing charge accumulation at the electrode ($x\rightarrow d$) the field lowering ΔE_{if} becomes more homogeneous. Hence, it is assumed that in the charge separation case the space charge profile ρ_x is not homogeneous. The electrostatic calculations presented above rather suggest a strong space charge accumulation ($a_i\rightarrow\infty$) at the interface between surface layer and electrode ($x\rightarrow d$).

In the case of charge injection where the space charges σ_{if} completely originate from the electrodes (i.e., $\rho_x=0$) an identical correlation between σ_{if} and $V_{c,\mathrm{shift}}$ is obtained as for the separation case with $a_i\rightarrow\infty$.

Thus, for both screening mechanisms, charge separation as well as injection, a correlation between the trapped interface charges σ_{if} and the voltage shift of the hysteresis loop, $V_{c,\mathrm{shift}}$, can be established. The calculations for the charge separation case indicate a strong charge accumulation at the interface between surface layer and electrode.

B. Screening mechanisms

In Ref. 4 it was shown that the driving force of imprint E_{if} is determined by the ferroelectric polarization and the interfacial and ferroelectric capacitance C_{if} and C_{fe}. In the previous section it has been shown that the trapped interface charges σ_{if} screen the field in the interface and, hence, lower E_{if} in the course of aging by $\Delta E_{if}(x,t)$:

$$E_{if}(x,t)=P_{\mathrm{fe}}\,\frac{A}{C_{if}+C_{\mathrm{fe}}}\,\frac{1}{\delta}-\Delta E_{if}(x,t). \tag{13}$$

Additionally, a correlation between the trapped interface charges and the voltage shift of the hysteresis loop has been established. In the following, different charge transport

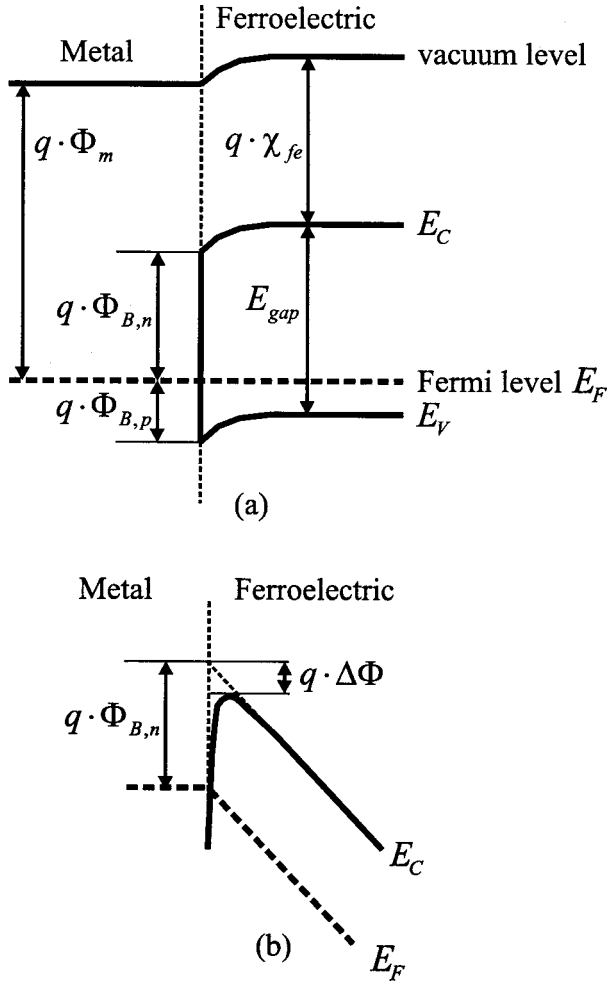

FIG. 4. (a) Sketch of the energy band matchup of a metal electrode-ferroelectric bilayer with the barrier for hole and electron injection $\Phi_{B,p}$ and $\Phi_{B,n}$. (b) Field assisted barrier lowering $\Delta\Phi$ according to the Schottky effect.

mechanisms according to different screening mechanisms are evaluated for the generation of the trapped interface charges σ_{if}:

$$\sigma_{if} = \int_0^t J(\tau)\, d\tau. \tag{14}$$

Using these correlations a numerical simulation is developed for the different screening mechanisms in order to compare the simulation results with experimental data.

1. Charge injection

As possible charge injection mechanisms Schottky emission and tunneling of electronic charges from the electrode into the thin film will be discussed. Usually, the electrode-ferroelectric structure is treated as a metal-insulator contact known from standard semiconductor textbooks (e.g. Ref. 13). In Fig. 4 the metal-ferroelectric energy band matchup is sketched.

The barrier height Φ_B is determined by the difference between the metal work function Φ_m and the electron affinity of the ferroelectric χ_{fe}. In the case of PZT and similar films the barrier height might differ from the ideal value proposed in semiconductor textbooks.[14] However, it is agreed that changing the top electrode metal (in this case of Au instead of Pt) results in a significant variation of the barrier height.[15,16] Values for the barrier height and electron affinity of particular electrode-ferroelectric material combinations can be found in Ref. 16. For the two potential transport mechanisms, Schottky emission and tunneling, which will be discussed in the following, this barrier height is a decisive parameter to modify the charge transport across this barrier.

For the Schottky emission which combines the thermionic emission with the barrier lowering according to the Schottky effect,[13] the current flow across the barrier Φ_B can be expressed as

$$J_S = A^{**} T^2 \exp\frac{-q\Phi_B}{kT} \exp\frac{q\Delta\Phi}{kT}, \tag{15}$$

where A^{**} is the effective Richardson constant, T the temperature, q the unit charge, k the Boltzmann constant, and $\Delta\Phi$ the barrier lowering due to the Schottky effect. The barrier lowering amounts to

$$\Delta\Phi = \sqrt{\frac{qE}{4\pi\epsilon}}, \tag{16}$$

where E denotes the field at the barrier as the cause for the barrier lowering and ϵ the dielectric constant of the barrier region. In this case the barrier lowering is caused by E_{if} and the permittivity is the optical permittivity in the surface layer, $\epsilon_{if,\mathrm{opt}}$, excluding the domain wall and ionic contributions to the dielectric constant. The optical permittivity in the denominator in Eq. (16) is used since the injected electrons or holes are hot charge carriers.[13,17] Their transition time across the barrier is too short in order to cause the aforementioned contributions to the dielectric constant. In case of Schottky emission being the cause of imprint, the field at the interface, E_{if}, is at a maximum in the initial state and in the course of aging E_{if} is gradually decreased by ΔE_{if} due to the trapped interface charges according to the calculations presented in Sec. II A. In the case of charge injection ($a_i \to \infty$) the field lowering ΔE_{if} is constant within the surface layer

$$\Delta E_{if}(t) = -\frac{A}{C_{if} + C_{\mathrm{fe}}} \frac{1}{\delta} \sigma_{if}(t). \tag{17}$$

On the other hand, the trapped interface charges σ_{if} can be calculated by the integration of the Schottky current J_S according to Eq. (15):

$$\sigma_{if}(t) = \int_0^t J_S(\tau)\, d\tau. \tag{18}$$

With the decrease of E_{if}, i.e., the increase of σ_{if}, $\Delta\Phi$ is reduced resulting in an increase of the effective barrier height, $\Phi_B - \Delta\Phi$, which leads to a reduction of the Schottky current density J_S in the course of aging. Hence, the charge transport across the barrier and the barrier lowering are interlinked.

Furthermore, the voltage shift, $V_{c,\mathrm{shift}}$, depends linearly on the trapped interface charges σ_{if} according to Eq. (12)

TABLE I. Parameters used for the numerical simulation of the evolution of $V_{c,\mathrm{shift}}$ shown in Fig. 5 according to the Schottky emission.

A^{**} (A/m^2K^2)	T (K)	$\epsilon_{if,\mathrm{opt}}$	P_{fe} ($\mu C/cm^2$)	$(C_{if}+C_{\mathrm{fe}})/A$ ($fF/\mu m^2$)
120×10^4	300	5	35	700

with $a_i \rightarrow \infty$. Thus, the voltage shift $V_{c,\mathrm{shift}}$ caused by Schottky emission can be calculated numerically using the equations introduced above [Eqs. (11)–(17)].

During the initialization the parameters used in the calculation are assigned to the initial values according to Table I. The numerical simulations were carried out for different barrier heights and different surface layer extensions δ. Additionally, independent experimental values for a 200 nm PZT film were used for the simulation [$P_{\mathrm{fe}}=35\,\mu C/cm^2$, $(C_{if}+C_{\mathrm{fe}})/A=700\,fF/\mu m^2$]. Figure 5(a) displays a simulation with a barrier height of $\Phi_b=1.2$ eV and a surface layer extension of $\delta=1$ nm. It can be seen that with this approach, the experimentally observed logarithmic time ($\log t$) dependence is obtained for this simulation. This indicates that the assumption of the reduction of the barrier lowering is a reasonable approach to describe the experimentally observed $\log t$ dependence. According to the Schottky emission, the charge transport across this barrier strongly depends on the barrier height Φ_B as can be seen in Fig. 5(b). The simulated evolution of the voltage shift is dramatically reduced due to an increase of the barrier height by 0.5 eV. In Fig. 5(c) the influence of the surface layer extension is displayed for a barrier height $\Phi_B=1.1$ eV. It can be seen that the extension δ significantly influences the evolution of the voltage shift. This significant influence can be understood since the field E_{if} in the interfacial layer in the initial is state ten times larger for an extension of 1 nm compared to that for 10 nm. This difference results in an initial barrier lowering $\Delta\Phi$ of 0.38 eV for a 1 nm extension compared to 0.12 eV for a 10 nm extension.

Figure 5(b) suggests that it can be verified whether the Schottky emission is a reasonable assumption as cause for the charge injection by modifying the barrier height Φ_B and hence, leads to the observed imprint effect. The barrier height can be modified by using different metal electrode materials with different work functions. In this case, a PZT film with gold top electrode and a platinum bottom electrode has been investigated. According to Sze, the workfunction of platinum amounts to 5.7 eV whereas for gold a value of 5.2 eV is reported for Φ_m.[13] Hence, by changing the metal workfunction by 0.5 eV, the barrier height Φ_B is changed by the same value and thus, the charge transport should be affected dramatically as is predicted by the simulation in Fig. 5(b). Therefore, the PZT capacitor with a gold top and a platinum bottom electrode should reveal a severe influence on the orientation of the polarization state which had been established. Depending on the orientation of the polarization, either the top or bottom interface should be decisive. Assuming electrons to be the injected species, imprint should be significantly more pronounced for gold top electrode in the case when P_{r-} is established. On the other hand, establishing P_{r+} should result in less pronounced imprint behavior

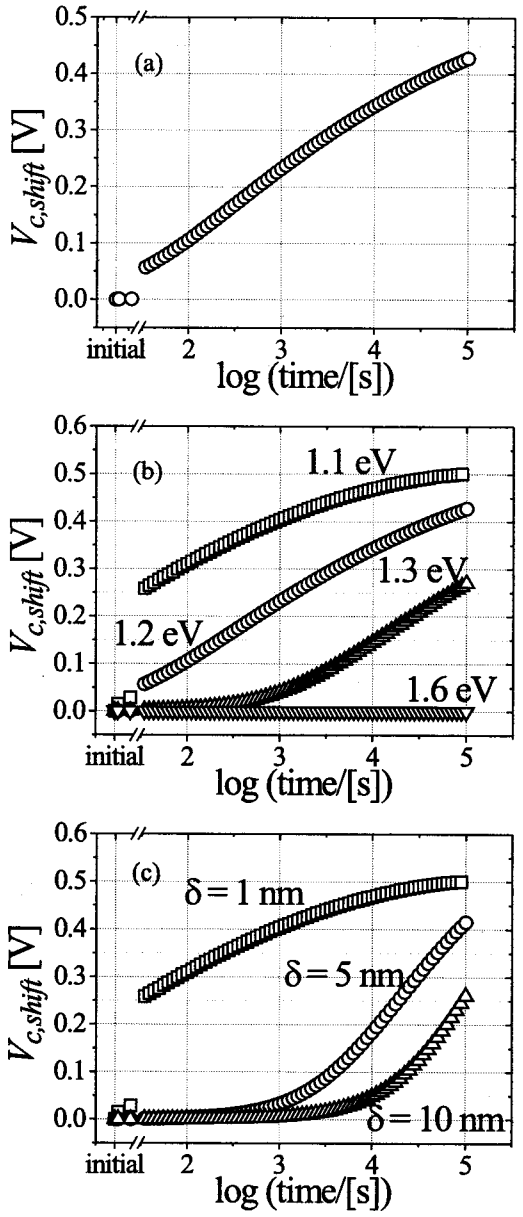

FIG. 5. (a) Numerical simulation of the evolution of $V_{c,\mathrm{shift}}$ reveals the experimentally observed $\log t$ dependence ($\Phi_B=1.2$ eV, $\delta=1$ nm). (b) Influence of the barrier height Φ_B on the simulated voltage shift evolution in the case of Schottky emission. (c) Influence of the surface layer extension δ on the voltage shift evolution ($\Phi_B=1.1$ eV).

since in that case the platinum bottom electrode interface is decisive. In the case of hole injection the polarity dependence would be vice versa but in any case, a strong polarity dependence should be observed.

In Fig. 6 the polarity dependence is displayed for a PZT film with a golden top and a platinum bottom electrode. No significant polarity dependence is observed. Since the polarity dependence predicted by the simulation for ferroelectric capacitors with different top and bottom electrode materials is not observed, it is concluded that the Schottky emission is not the dominant mechanism to explain imprint.

For the second injection mechanism, tunneling, the bar-

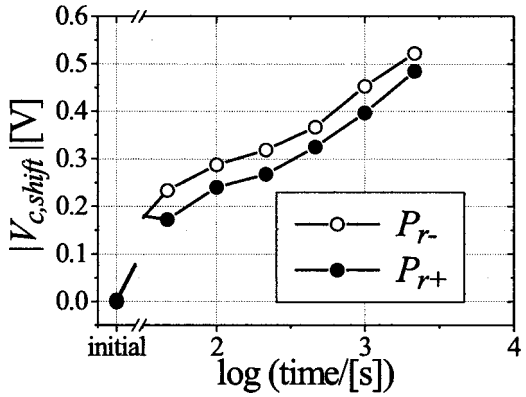

FIG. 6. Polarity dependence (P_{r+} and P_{r-} established) of imprint on a PZT film with different top (Au) and bottom (Pt) electrode material (at room temperature).

rier height is also a decisive parameter for the tunneling current.[13] The tunneling current J_T is

$$J_T = \text{const}\, E^2 \exp\left[-\frac{4\sqrt{2m^*}(q\Phi_B)^{3/2}}{3q\hbar E}\right], \tag{19}$$

where m^* is the effective mass and $\hbar$ the reduced Planck constant.

Evaluating Eq. (19) as the origin for imprint would result in a similar polarity dependence for ferroelectric capacitors with different top and bottom electrode materials as predicted for Schottky emission [see simulation in Fig. 5(b)]. In the case of tunneling, the polarity dependence should be even more pronounced since the exponent in Eq. (19) includes $\Phi_B^{3/2}$ instead of Φ_B for the Schottky emission [Eq. (15)]. However, the simulation shown in Fig. 5(b) demonstrates clearly that an exponential expression similar to Eq. (19) is very sensitive to the exponent and hence, a significant polarity dependence should be observed in the case of tunneling. However, according to Fig. 6, ferroelectric capacitors with different top and bottom electrode materials and thus different barrier heights reveal no significant polarity dependence.

Although a charge injection mechanism is very promising to explain several experimental observations on ferroelectric thin films such as size effects,[18] fatigue,[19] and electronic conduction,[7] the results and simulations presented in this section indicate that charge injection from the electrode into the thin film, either caused by Schottky emission or by tunneling, is not the dominant cause for imprint in ferroelectric thin films.

2. Charge separation

The electric field in the surface layer E_{if} can also cause charge separation within this layer presumably caused by changes of valency of defect or regular ions within the layer. The Frenkel–Poole emission displayed in Fig. 7 could be responsible for charge separation in the surface layer.[13] This emission is due to a field-enhanced thermal excitation of trapped electrons or holes into the conduction band or valence band, respectively. For trap states with Coulomb potential, the expression for the charge transport according to the Frenkel–Poole emission is very similar to the one for Schottky emission [Eq. (15)].

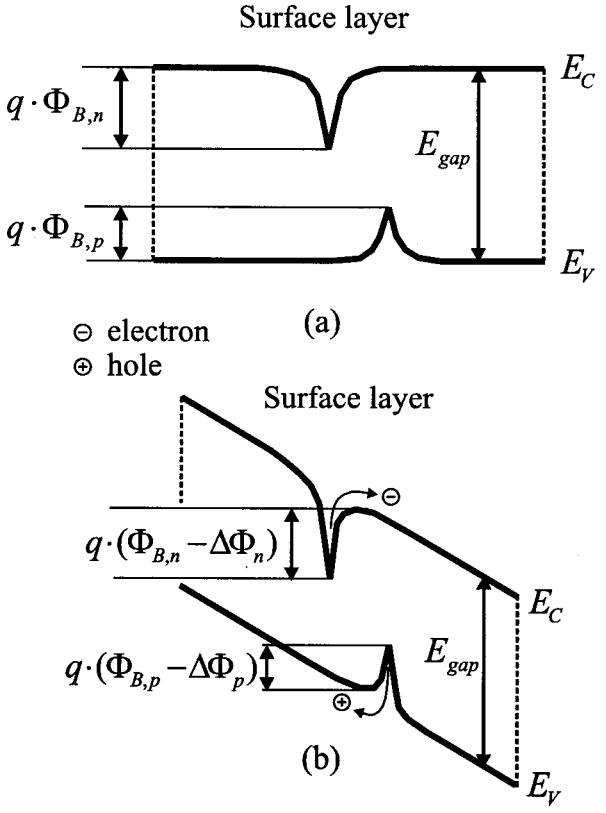

FIG. 7. Sketch of the Frenkel–Poole emission of trapped electrons and holes. (a) No electric field present in the layer and (b) electric field leads to a barrier lowering by $\Delta\Phi_p$ for holes and $\Delta\Phi_n$ for electrons.

The barrier height Φ_B in the Frenkel–Poole case describes the depth of the potential well. The current flow according to the Frenkel-Poole emission can be expressed as

$$J_{\text{FP}} = \sigma_{\text{FP}} E \exp\frac{-q\phi_B}{kT} \exp\frac{q\Delta\phi}{kT}. \tag{20}$$

The prefactor σ_{FP} in Eq. (20) describes a conductivity. It is a function of the density of the trapping centers, the mobility of the emitted charge carriers, and other parameters.[20] It is generally assumed that σ_{FP} is a constant with respect to the electric field.[20–22] Sze assumes σ_{FP} also to be temperature independent in the case of silicon nitride films[22] while Pulfrey and co-workers also include temperature dependent parameters to describe σ_{FP} Ref. 20 in a theoretical discussion of electronic conduction in insulating films. The second exponential expression again describes the barrier lowering caused by the electric field

$$\Delta\Phi = \sqrt{\frac{qE}{\pi\epsilon}}. \tag{21}$$

The barrier lowering in the case of Frenkel–Poole emission differs by a factor of 2 from the one for Schottky emission [see Eq. (16)] due to the immobility of the ionic center which emits the electronic charge.[13] By performing similar numerical calculations as for the Schottky emission in the previous

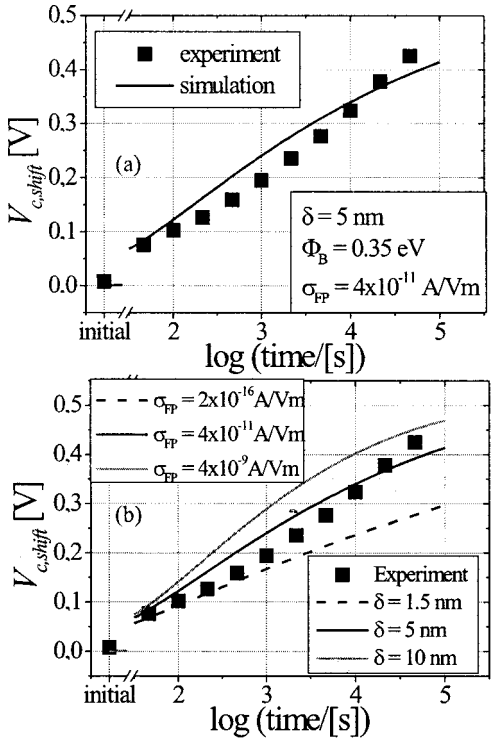

FIG. 8. (a) Experimental data (symbols, PZT 30:70, 200 nm, room temperature) and numerical simulation of the voltage shift evolution (line). A good match is obtained for the parameters as given in the figure. (b) Influence of the surface layer extension δ on the voltage shift ($\Phi_B = 0.35$ eV). The prefactor σ_{FP} was adjusted as indicated in the figure.

section, the evolution of the voltage shift caused by a Frenkel–Poole effect within the surface layer can be simulated. The prefactor σ_{FP} has been assumed constant with respect to electric field and temperature.

Figure 8(a) displays experimental data and a simulation of the voltage shift caused by the Frenkel–Poole effect. Assuming Frenkel–Poole emission within the surface layer gives a reasonable agreement between experiment and simulation. In good approximation the experimentally observed $\log t$ dependence is obtained for the simulation. The parameters used for the simulation are given in Table II. The value used for the sum of the interfacial capacitance C_{if} and C_{fe} was chosen to be 700 fF/μm^2, as determined experimentally.

Figure 8(b) shows the influence of the surface layer extension δ on the evolution of the voltage shift. The barrier height Φ_B in all cases was 0.35 eV. The prefactor σ_{FP} had to be adjusted in order to obtain a good agreement between experiment and simulation. The values used for σ_{FP} in the simulation are given in Fig. 8. It can be seen that the surface layer extension influences the slope of the voltage shift evolution. The best fit is obtained for an extension of approximately $\delta = 5$ nm. Using the values determined experimentally for C_{if} and C_{fe} in Ref. 4 for the same film which provided the experimental data shown in Fig. 8, the value of the dielectric constant in the surface layer can be estimated and compared to the one in the ferroelectric layer. Using 5 nm for the surface layer extension δ yields a dielectric constant $\epsilon_{if} \approx 400$ ($C_{if} \approx 700$ fF/μm^2) whereas the dielectric constant of the ferroelectric layer is approximately 600 ($C_{\mathrm{fe}} \approx 27$ fF/μm^2, film thickness 200 nm). The decrease of the dielectric constant in the surface layer compared to the undisturbed ferroelectric region seems to be reasonable since the surface layer is assumed to be a distorted layer with inferior ferroelectric and electrical properties compared to those of the ferroelectric layer. In the following, additional experimental results will be compared to the predictions of the interface screening model according to a Frenkel–Poole type charge separation mechanism.

TABLE II. Parameters used for the numerical simulation of the evolution of $V_{c,\mathrm{shift}}$ shown in Fig. 8 according to the Frenkel–Poole emission.

T (K)	$\epsilon_{if,\mathrm{opt}}$	P_{fe} (μC/cm^2)	$(C_{if}+C_{\mathrm{fe}})/A$ (fF/μm^2)
300	5	35	700

3. Comparison with experimental results

In the following, experimental results will be compared to the simulations of the interface screening model. It has already been shown that the improvement of the imprint behavior of PZT films with thin $SrRuO_3$ layers at the electrodes can be understood with the proposed model.[23] In literature an increase of the interfacial capacitance C_{if} has been reported[24,25] due to the use of oxide electrodes. With this increase of C_{if} an improvement of imprint can be understood since C_{if} influences the driving force of imprint, E_{if}, as well as the correlation between trapped charges, σ_{if}, and the voltage shift, $V_{c,\mathrm{shift}}$, since it can be found in both expressions in the denominator [see Eqs. (12) and (13)]. Now, the thickness and temperature dependence of imprint will be evaluated.

a. Thickness dependence In Fig. 9(a) experimental data (symbols) are shown for imprint measurements on PZT films with varying sample thickness in the range between 100 and 300 nm. Imprint is clearly more pronounced with increasing film thickness. The simulations (lines) are plotted in the same graph. In Fig. 9(b) the corresponding hysteresis loops are displayed for the PZT films with different thickness. The remanent polarization P_r slightly decreases upon decreasing sample thickness [$P_r(100\,\mathrm{nm}) \approx 22\,\mu$C/cm^2, $P_r(200\,\mathrm{nm}) \approx 27.5\,\mu$C/cm^2, $P_r(300\,\mathrm{nm}) \approx 31.5\,\mu$C/cm^2]. For the same PZT thickness series, the interfacial capacitance was determined experimentally ($C_{if} \approx 700$ fF/μm^2). The ferroelectric capacitance depends on the film thickness ($C_{\mathrm{fe}}(100\,\mathrm{nm}) \approx 39$ fF/μm^2, $C_{\mathrm{fe}}(200\,\mathrm{nm}) \approx 26$ fF/μm^2, $C_{\mathrm{fe}}(300\,\mathrm{nm}) \approx 13$ fF/μm^2). With these experimentally determined values (P_r, C_{fe}, and C_{if}) the evolution of the voltage shift was simulated according to the equations introduced above [Fig. 9(a)]. A reasonable agreement is obtained between experiment and simulation even for this simple approach by changing only the values for P_{fe} and C_{fe}.

b. Temperature dependence In Fig. 10 imprint measurements performed at different temperatures (symbols) and the corresponding numerical simulations (lines) are shown. A good agreement between experiment and simulation is obtained for a depth of the potential well of 0.35 eV. In that case the extension of the surface layer δ was chosen to be temperature dependent and δ increases linearly with tem-

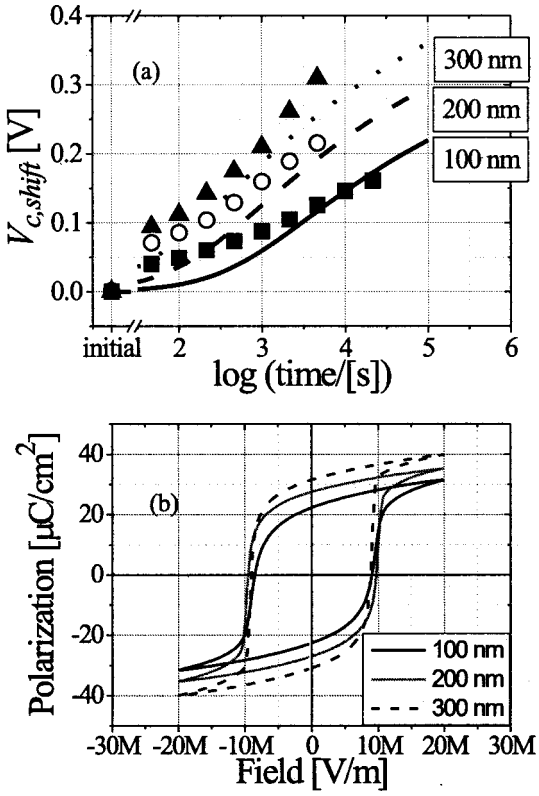

FIG. 9. (a) Imprint behavior (experiment: symbols, simulation: lines) of PZT (30:70) films with different film thickness. (b) Corresponding hysteresis measurements (room temperature).

perature. An increase of the surface layer extension in the course of aging was experimentally verified for fatigue measurements[24] and also for aging of PZT films.[26] It was also shown that the growth of the surface layer extension δ seems to be more pronounced at higher temperatures.[26] Hence, the assumption of a variation of δ with temperature seems to be reasonable for the simulations. In the case of the numerical simulations shown in Fig. 10 a constant value of δ was assumed for the different temperatures as given in Table III. The permittivities in the surface layer ϵ_{if} and the ferroelectric layer ϵ_{fe} were assumed to be temperature independent ($\epsilon_{if}=400$, $\epsilon_{\mathrm{fe}}=600$, as estimated in the previous section). The value of the prefactor σ_{FP} in the case of the simulations for the PZT film shown in Fig. 10 amounted to 4×10^{-11} A/V m.

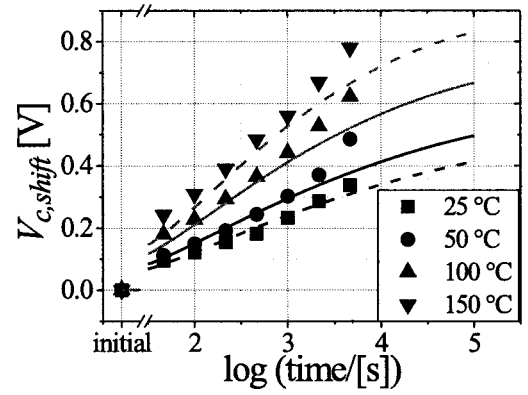

FIG. 10. Imprint measurements performed at four different temperatures (symbols, PZT, 20:80, 200 nm) and the corresponding numerical simulations according to the Frenkel–Poole mechanism (lines). The following parameters were used for the simulation: $\Phi_B=0.35$ eV, $\delta=f(T)$ according to Table III, and $\sigma_{\mathrm{FP}}=4\times10^{-11}$ A/V m.

TABLE III. Values of the extension of the surface layer δ used for the numerical simulation of the evolution of $V_{c,\mathrm{shift}}$ as a function of the temperature. A linear correlation between δ and the temperature is assumed. Experiment and simulation are shown in Fig. 10.

	$T=25$ °C	$T=50$ °C	$T=100$ °C	$T=150$ °C
δ (nm)	5	5.7	7.2	8.7

In the case of silicon nitride films, Sze estimates a value for σ_{FP} on the order of 10^{-3} A/V cm and a depth of the potential well Φ_B of 0.64 eV from the slope of the Frenkel–Poole current in the Arrhenius plot.[22] In the case of PZT films investigated in this work, the simulations of imprint measurements reveal a significantly smaller value for σ_{FP} (see Fig. 10). However, σ_{FP} has to exceed the total conductivity of the PZT film. Otherwise, σ_{FP} would control the overall conductivity of the PZT film. The total conductivity of this film determined by leakage current measurements is approximately two orders of magnitude smaller than σ_{FP}. Hence, the estimated value of σ_{FP} for PZT seems to be reasonable.

However, the assumption that only the Frenkel–Poole mechanism contributes to imprint even at elevated temperatures might introduce a slight deviation from the real situation since at elevated temperatures other processes with higher activation energies might get involved (e.g., defect dipole alignment) in the contribution to imprint.

Robertson reports relatively shallow traps with small activation energies for regular ions in SBT and PZT thin films.[9–11] The valency changes of these regular ions could be the cause for imprint in ferroelectric thin films. But also valency changes of defect or surface states are conceivable as the origin of the trapped charges in the imprint scenario.

III. CONCLUSION

In this article the imprint behavior of ferroelectric PZT films has been theoretically discussed. Numerical simulations based on the interface screening model for different screening mechanisms, charge injection as well as charge separation within the surface layer, were implemented. The simulation results based on charge injection predict a strong dependence of imprint on the electrode material. Since this dependence is experimentally not observed it is concluded that charge injection from the electrode into the thin film is not the dominant imprint mechanism in ferroelectric thin films. The simulation results for a Frenkel–Poole type charge separation mechanism within the surface layer give a reasonable agreement between experiment and simulation. With the proposed model the time, thickness, and temperature dependence of imprint can be quantitatively understood. A good agreement between experiment and simulation is obtained for shallow traps (0.35 eV) and a surface layer extension of approximately 5 nm.

ACKNOWLEDGMENTS

The authors would like to acknowledge Professor G. Arlt from the University of Aachen, and R. Bruchhaus, N. Nagel, W. Hartner, G. Schindler, and M. Kastner from Infineon Technologies for fruitful discussions. Furthermore, the authors are indebted to T. Schneller and R. Gerhardt for providing the PZT films and S. Tiedke and T. Schmitz for their support in electrical characterization. This work was supported by the German Ministry of Education and Research BMBF (Contract No. 03N60075).

[1] S. Eaton, D. Butler, M. Parris, D. Wilson, and H. McNeillie, Dig. Tech. Pap.-IEEE Int. Solid-State Circuits Conf. (1988), p. 130.
[2] J. Scott and C. P. de Araujo, Science **246**, 1400 (1989).
[3] C. P. de Araujo, J. Cuchiaro, L. McMillan, M. Scott, and J. Scott, Nature (London) **374**, 627 (1995).
[4] M. Grossmann, O. Lohse, D. Bolten, U. Boettger, T. Schneller, and R. Waser, J. Appl. Phys. **92**, 2680 (2001).
[5] T. Mihara and H. Watanabe, Jpn. J. Appl. Phys., Part 1 **32**, 5664 (1995).
[6] T. Mihara and H. Watanabe, Jpn. J. Appl. Phys., Part 1 **32**, 5674 (1995).
[7] I. Stolichnov and A. Tagantsev, J. Appl. Phys. **84**, 3216 (1998).
[8] H.-M. Chen and Y.-M. Lee, Appl. Phys. Lett. **73**, 309 (1998).
[9] J. Robertson, W. Warren, B. Tuttle, D. Dimos, and D. M. Smith, Appl. Phys. Lett. **63**, 1519 (1993).
[10] J. Robertson, W. Warren, and B. Tuttle, J. Appl. Phys. **77**, 3975 (1995).
[11] J. Robertson, C. W. Chen, W. Warren, and C. D. Gutleben, Appl. Phys. Lett. **69**, 1704 (1996).
[12] K. Watanabe, A. Hartmann, R. Lamb, R. Craig, M. Thurgate, and J. Scott, Jpn. J. Appl. Phys., Part 2 **39**, L309 (2000).
[13] S. M. Sze, *Physics of Semiconductor Devices* (Wiley, New York, 1981).
[14] I. Stolichnov, A. Tagantsev, N. Setter, J. Cross, and M. Tsukada, Appl. Phys. Lett. **75**, 1790 (1999).
[15] G. Dietz, W. Antpohler, M. Klee, and R. Waser, J. Appl. Phys. **78**, 6113 (1995).
[16] J. Scott, K. Watanabe, A. Hartmann, and R. Lamb, Ferroelectrics **225**, 83 (1999).
[17] G. W. Dietz, Ph.D. thesis, RWTH Aachen, 1997.
[18] A. Tagantsev and I. Stolichnov, Appl. Phys. Lett. **74**, 1326 (1999).
[19] I. Stolichnov, A. Tagantsev, E. Colla, and N. Setter, Appl. Phys. Lett. **73**, 1361 (1998).
[20] D. Pulfrey, A. H. M. Shousha, and L. Young, J. Appl. Phys. **41**, 2838 (1970).
[21] I. T. Johansen, J. Appl. Phys. **37**, 499 (1966).
[22] S. Sze, J. Appl. Phys. **38**, 2951 (1967).
[23] M. Grossmann, O. Lohse, T. Schneller, D. Bolten, U. Boettger, J. Rodriguez, H. Kohlstedt, and R. Waser, Int. Ferroelectrics (in press).
[24] J. Lee, C. Thio, M. Bhattacharya, and S. Desu, Mater. Res. Soc. Symp. Proc. **261**, 241 (1995).
[25] S. Desu and O. Vendik, Integr. Ferroelectr. **28**, 175 (2000).
[26] M. Grossmann, O. Lohse, D. Bolten, U. Boettger, T. Schneller, and R. Waser, Appl. Phys. Lett. **80**, 1427 (2002).